Int. J. Electrochem. Sci., 15 **(2020)** 2261 – 2271, doi: 10.20964/2020.03.07

International Journal of
ELECTROCHEMICAL
SCIENCE
www.electrochemsci.org

Corrosion Behavior of X80 Steel Under Anodic Polarization

Su Xibeier[1], *Wang Wenwu*[1,*], *Wang Lei*[2], *Yu Hao*[3]

[1] Liaoning Shihua University College of Petroleum Engineering, Fushun, China, 113001
[2] No.1 Pipeline Company, China Petroleum Pipeline Engineering Co., Ltd., Langfang, China, 065000
[3] Petrochina Henan Gas & Marketing Company, Zhengzhou, China, 450000
[*]E-mail: wwenwu_pet@163.com

Received: 3 November 2019 / *Accepted:* 15 December 2019 / *Published:* 10 February 2020

To investigate the corrosion behavior of X80 steel caused by an anodic current density, electrochemical tests of X80 steel in near-natural NS4 solution under varying anodic current densities, I_{ac}, were performed. The testing combined a three-electrode and direct-current source. Analysis included electrochemical testing and corrosion morphology. The results show that the corrosion behavior of X80 steel in NS4 solution is mainly divided into two stages. The first stage, I_{ac}=0~20mA/cm^2, was characterized by the formation of a double electric layer and a corrosion-product layer mainly comprised of FeOOH. During this stage uniform corrosion occurs and I_{corr} increases linearly. In the second stage where $I_{ac}\geq$50mA/cm^2, the corrosion morphology is pitting corrosion and I_{corr} is basically unchanged. Black Fe_3O_4 is the primary inner layer corrosion product that inhibits uniform corrosion and promotes pitting corrosion.

Keywords: Anodic polarization; X80 steel; Polarization curve; EIS; Corrosion morphology

1. INTRODUCTION

High voltage direct current (HVDC) transmission systems are commonly in bipolar symmetric connection mode [1]. During normal operation, the leakage current into the soil is less than 1%. However, during system malfunctions, the systems changes to single mode resulting in soil currents that can reach thousands of amperes that can significantly affect buried metal facilities [2]. Focusing on the severity of the interference of HVDC, Nicholson found HVDC fault current flows into buried pipeline, lasting for several days along the pipeline until outflowing causing serious corrosion [3]. Based on the field test, the current density leaving the pipe can reach 82mA/cm^2. Under this condition, research has analyzed the influence of cathodic polarization [4,5] on an anti-corrosion coating and determined the criterion for cathodic protection.

Compared to direct stray current (DC), more literature focuses on its corrosion rate, product, mechanism and model of alternating stray current (AC), and a comprehensive understanding has been in consensus [6]. However, based on the regulation that DC corrosion rate conforms to Faraday's law, few researches have been conducted on its corrosion behavior, even though corrosion rate resulted by DC is much larger than that of AC. Furthermore, corrosion becomes more severely with the development of HVDC. Results we got preliminary based on simulation and field test show the peak of current density at defects on coatings can reach 100A/m^2, which may cause the rapid perforation of pipeline [7]. It is interesting that at some points current flows out into soil, the surface of defects is covered with a layer of dense products, which prevents the later soil corrosion.

However, there are few studies on the effect of anodic polarization, that is, outflowing current on corrosion potential or morphology of buried pipeline. In this paper, based on the conventional electrochemical system with three-electrodes, the electrochemical method was applied to explore the corrosion behavior of X80 steel under anodic current densities in the range of 0~100 mA/cm^2.

2. EXPERIMENTAL SECTION

Fig.1 shows the diagram for the electrochemical test for X80 steel with applied anodic current density. In this system, the direct-current source was used to provide anodic current to act on the X80 steel and the electrochemical station was used for measuring open-circuit potential, polarization curves, and the EIS (electrochemical impedance spectrum) of X80 steel under varying anodic current densities. The X80 steel in 10×10×2mm^3 and works as a working electrode, the reference electrode is a saturated calomel electrode (SCE) and the auxiliary electrode is a Pt electrode. The reference electrode is in contact with the solution through a Lugin capillary, and the distance between the tip and the surface of X80 steel is less than 2mm to ignore the IR drop of the solution.

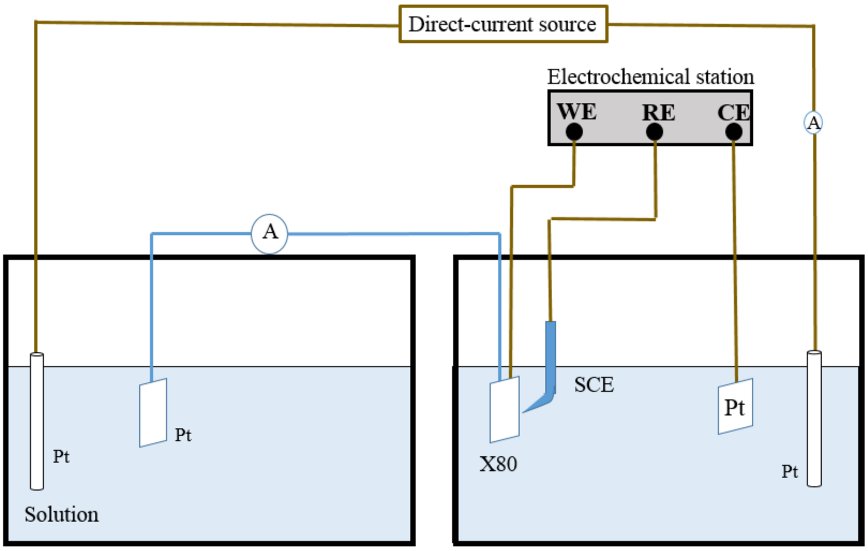

Figure 1. The diagram of electrochemical test for X80 steel under the conditions of anodic current density (0~100 mA/cm^2) in near-neutral NS4 soil-simulation solution (pH=7.2)

The experimental solution in this paper is near-neutral NS4 soil-simulation solution with $NaHCO_3$ 0.483, KCl 0.122, $CaCl_2$ 0.137, $MgSO_4 \cdot 7H_2O$ 0.131 in g/L, and 5% CO_2/N_2 was used to move the oxygen and to maintain a pH=7.2.

The TAFEL curve obtained by the electrochemical station was tested with a scanning rate of 0.3mV/s, and a potential range of ±250 mV (vs. open-circuit potential). The scanning range of EIS was 100kHz~10mHz. All the tests were performed in a constant temperature humidity chamber (GDJS-408). All experiments were repeated at least twice to ensure the accuracy [8].

3. RESULTS AND DISCUSSION

3.1 Analysis of corrosion kinetic parameters

Fig. 2 shows the variation of open-circuit potential of X80 steel under different anodic current densities. It can be seen that the open-circuit potential of X80 steel in NS4 solution is approximately -665.5$mV_{vs.SCE}$ without anodic current and as the anodic current density (I_{ac}) increases in the range 0~75mA/cm^2, the open-circuit potential of X80 steel increases linearly [9]. The results show that X80 steel is more inclined to an activated corrosion state at this time. The is mainly due to the anodic polarization of the working electrode resulting from the increased of outflow current density. However, as I_{ac} is further increased in the range 75~100mA/cm^2, the open-circuit potential remains basically unchanged, which may be the result of compact corrosion products covering the surface of X80 at I_{ac}=100mA/cm^2.

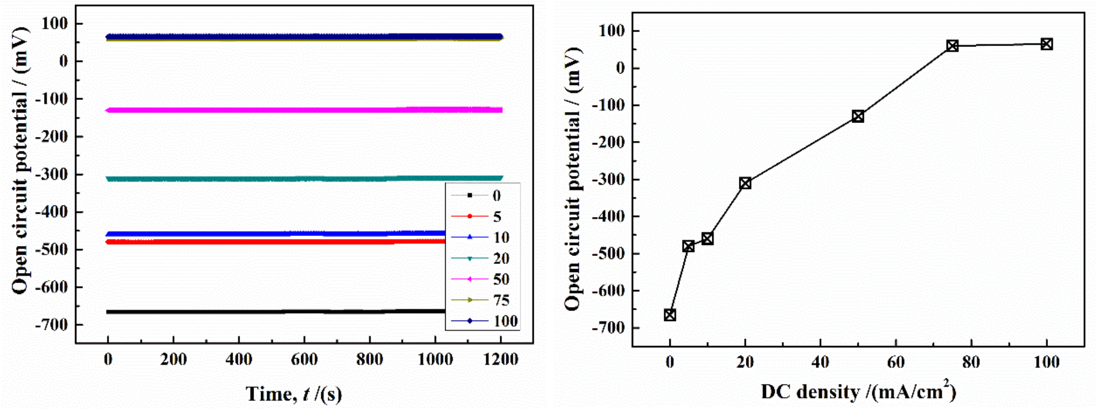

Figure 2. The variation of open-circuit potential of X80 steel under different anodic current densities (0~100 mA/cm^2) in NS4 solution

Fig.3 shows the potentiodynamic polarization curves of the test results of X80 steel under different anodic current densities and the fitted results are shown in Tab.1. It can be seen that anodic current makes the polarization curve move to the upper right, which means the corrosion potential, E_{corr}, continues to move positively as I_{corr} increases, and there is no obvious passivation region.

The cathodic and anodic Tafel slopes, b_a and b_c respectively, are used to describe the influence of the polarization process. From the fitted results in Tab. 1, it can be seen that the ratio of $\beta = b_a/b_c$ is always less than 1, indicating that the anodic current mainly affects the cathodic process of X80 instead of the anodic process. Also from Fig. 3, in the region I_{ac}=0~20mA/cm^2, the cathodic polarization curve of X80 steel shows an obvious limiting-current diffusion control process. As I_{ac} increases, the ratio of β increases gradually in the range I_{ac}=20~75mA/cm^2 and remains relatively unchanged in the range I_{ac}=75~100mA/cm^2. The relationships described above may be related to the formation and destruction of corrosion products on the surface of X80 steel.

The corrosion potential has a linear relationship with anodic current density in the range I_{ac}=0~75mA/cm^2 and remains relatively unchanged in the range I_{ac}=75~100mA/cm^2. This agrees with the results of the open-circuit potential. However, the corrosion current density increases linearly in the range of I_{ac}=0~50mA/cm^2 before holding constant in the range of I_{ac}=50~100mA/cm^2 [10].

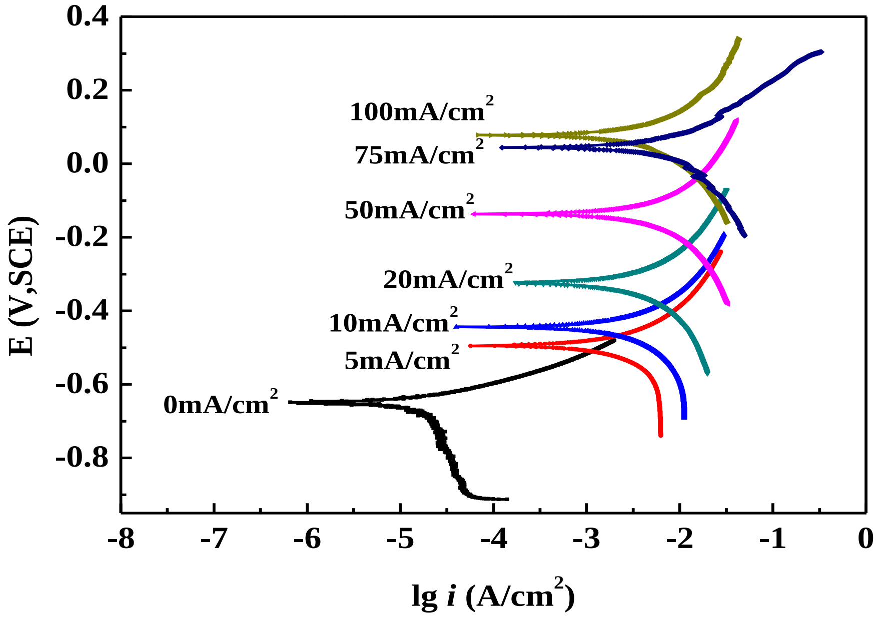

Figure 3. Potentiodynamic polarization curves of X80 steel under different anodic current densities (0~100 mA/cm^2) in NS4 solution

Table 1. Fitted results of polarization curves of X80 steel under different anodic current densities (0~100 mA/cm^2) in NS4 solution

I_{ac} (mA/cm^2)	E_{corr} (mV$_{vs.SCE}$)	b_a (mV)	b_c (mV)	β=b_a/ b_c	I_{corr} (mA/cm^2)
0	-651	72	690	0.104	0.02
5	-482	315	2456	0.128	6.29
10	-425	592	2715	0.218	16.48
20	-322	714	2291	0.312	24.76
50	-99	1683	2770	0.607	66.27
75	72	1201	1961	0.612	60.92
100	72	1539	3231	0.476	62.84

This happens because when there is no anodic interference, the diffusion process of the corrosion products on the metal surface is primarily related to the concentration of the metal surface products and the concentration of the surrounding solution, characterized by "free" diffusion, and with the increase of anodic current density, the concentration of the ions on surface increases rapidly allowing ions to move according to the direct current electric field [11]. At low anodic current density, the diffusion rate of corrosion products increases linearly, leading to a linear increase in corrosion current density. Once I_{ac}>50mA/cm^2, the diffusion rate of corrosion products saturates, and hence, the apparent corrosion current density also saturates.

3.2 Analysis of EIS

Fig. 4 shows the Nyquist diagram of X80 steel without anodic current. When the X80 is immersed in the NS4 solution, there is no adsorbed phase on the surface of the metal electrode, which means there is only one time constant [12]. Therefore, the equivalent electric circuit (EEC) is composed of solution resistance R_s, a double layer capacitance C and charge transfer resistance R_{ct}. Under the consideration of the dispersion effect, the pure capacitance of C is always replaced by constant phase angle element Q. Therefore, the EEC can be described as $R_s(R_{ct}Q_{dl})$.

Fig. 5 shows the EIS of X80 steel under different anodic current densities. It can be seen that when I_{ac}=5~20mA/cm^2, the Nyquist diagram shows a double capacitive arc, and there are two peaks in the Bode plot, indicating that there are two time constants in the process [13,14].

According to related research, under conditions of low anodic current densities, the corrosion reaction is controlled by the diffusion of corrosion products. To our best knowledge, the finite layer on the surface typically behaves as double capacitive-resistance arcs at an order of magnitude of 10^{-4} F/cm^2. Therefore, the EEC of the diffusion layer can be described as a series circuit of diffusion resistance R_c and diffusion capacitance C. The EEC of the whole system can be described as $R_s(Q_{dl}(R_{ct}(R_cC)$, including solution resistance R_s, charge transfer resistance R_{ct} and double layer capacitance Q_{dl},.

The capacitance of electric double layer can be calculated by the following Eq.(1):

$$Q_{dl} = \frac{\varepsilon A}{l} \tag{1}$$

In Eq.(1), l is the thickness of electric double layer, ε is the dielectric constant of solution, and A is the area of working electrode of 1cm^2.

In this paper, Q_{dl} and l are inversely proportional because ε and A are constant. Under these conditions, as I_{ac} increases, the R_{ct} decreases while Q_{dl} increases. The main reason for this is that the increase of I_{ac} makes the electric field force stronger, resulting in a decrease in the thickness of the electric double layer. The time constant of $\tau_1=R_{ct}\cdot Q_{dl}$ also decreases leading to an increase in the diffusion rate of ions in the electric double layer, that is, the reaction rate of $Fe \rightarrow Fe^{2+}$ increases. However, the R_c increases and C decreases. This is because the diffusion rate of corrosion products is lower than the formation rate, leading to an increase in the thickness of the diffusion layer that decreases C. Also, the difference in concentration of corrosion layer and solution is larger as I_{ac} increases, so the R_c increases. The time constant of $\tau_2=R_c\cdot \mathrm{C}$ decreases, indicating that the diffusion rate of corrosion products increases

[15].

When I_{ac}≥50mA/cm^2, the effects of the double capacitive reactance disappear. Under this condition the formation rate of corrosion products is equal to the diffusion rate, and this maintains a steady corrosion-product layer, leading to the disappearance of diffusion resistance R_c and diffusion capacitance C [16,17]. Therefore, the EEC can be described as $R_s(Q_{dl}R_{ct})$. In Fig.6, the charge transfer resistance of R_{ct} and the double layer capacitance of Q_{dl} are mostly unchanged in the region I_{ac}≥50mA/cm^2. This results in an unchanging time constant, τ_1, indicating a stable diffusion layer and double electric layer have been formed. In Fig.5(3) of log *f* - |Z|, in the range I_{ac}=0~100mA/cm^2, it can be divided into two stages. In first stage, I_{ac}=0~20mA/cm^2, the electric double layer and corrosion-product layer are gradually formed. In second stage, I_{ac}≥50mA/cm^2, the whole system is in steady state and is not affected by the anodic current density.

In EIS, resistance |*Z*| is dominated by mass transfer resistance at low-frequency and charge transfer resistance at high-frequency. It can be seen from Fig.5(3) that the mass transfer resistance performs obvious difference, especially when *f*=0.01Hz that has a positive relation with I_{ac} [18]. With I_{ac} increasing, the mass transfer resistance decreases while charge transfer resistance changes little. The results show that the diffusion process is controlled by charge transfer in the range I_{ac}=0~100mA/cm^2 [19,20]. The analyzed results are in good agreement with the polarization curves.

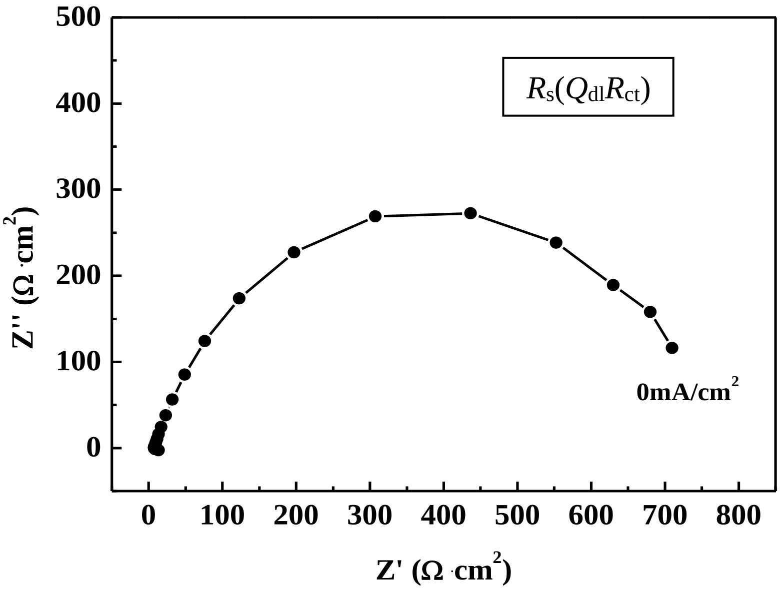

Figure 4. Nyquist diagram of X80 steel without anodic current in NS4 solution

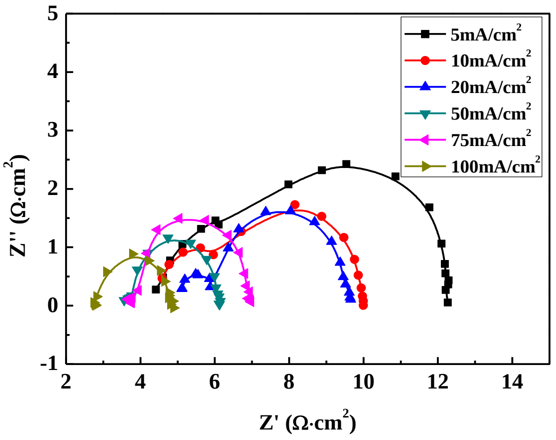

(1) Nyquist diagram

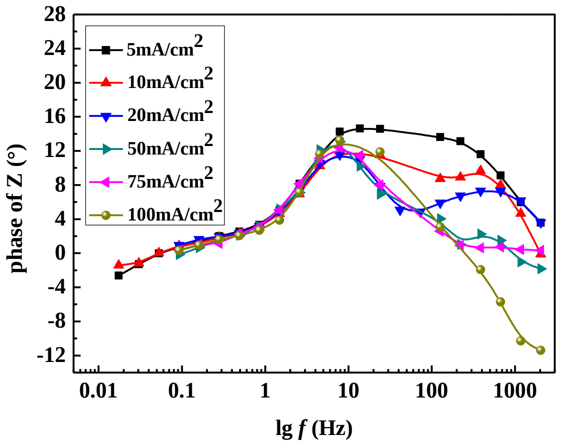

(2) Bode plots

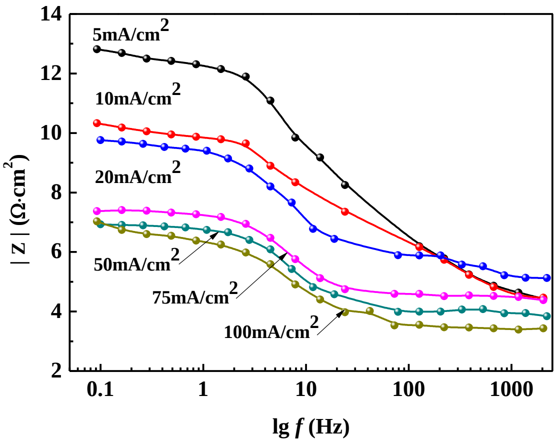

(3) log *f* - |*Z*|

Figure 5. EIS of X80 steel under different anodic current densities (0~100 mA/cm^2) in NS4 solution

Table 2. Fitted results of EIS of X80 Steel under different anodic current densities (0~100 mA/cm^2) in NS4 solution

I_{ac} (mA/cm^2)	R_{ct} ($\Omega\cdot$cm^2)	Q_{dl} (S$^n\cdot$cm^{-2})	τ_1 (10^{-2})	n	C (F$\cdot$cm^{-2})	R_c ($\Omega\cdot$cm^2)	τ_2 (10^{-4})
0	768.8	0.00073	56	0.785	-	-	-
5	5.893	0.0057	3.36	0.793	0.000260	2.116	5.5
10	3.636	0.0075	2.7	0.909	0.000277	1.909	5.3
20	2.606	0.0100	2.6	0.929	0.000325	1.016	3.3
50	2.303	0.0098	2.3	0.989	-	-	-
75	2.186	0.0094	2.1	0.968	-	-	-
100	2.161	0.0104	2.2	0.900	-	-	-

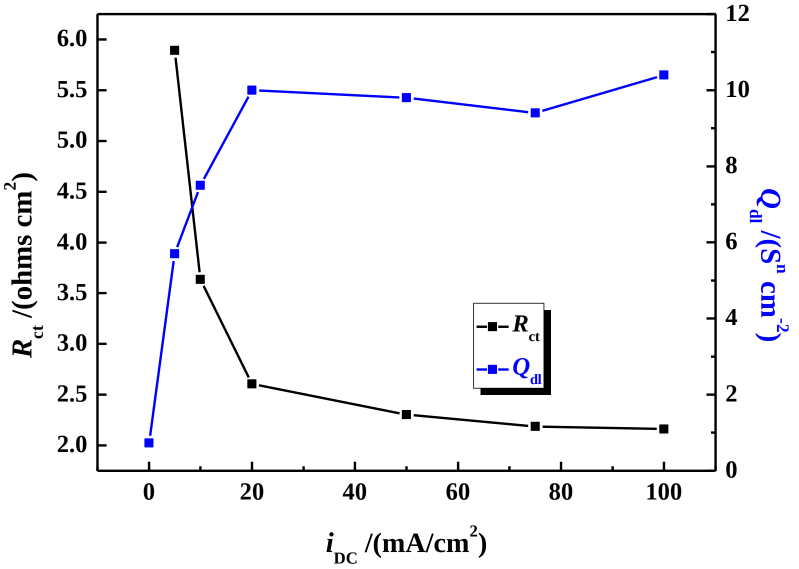

Figure 6. Change of R_{ct} and Q_{dl} of X80 steel under different anodic current densities (0~100 mA/cm^2) in NS4 solution

3.3 Analysis of corrosion morphology

Fig. 7 shows the corrosion morphology of X80 steel under different anodic current densities. It can be seen that with the increase of anodic current density, the inhomogeneity of the surface rapidly increases. When I_{ac}<20mA/cm^2, the corrosion rate is basically proportional to the anodic current density, and the roughness of surface slightly increases experiencing uniform corrosion. However, at an increased anodic current density of 50mA/cm^2, cracks begin to appear on the surface and its surface inhomogeneity rapidly increases. When the anodic current density is further increased to 75mA/cm^2~100mA/cm^2, there are obvious corrosion pits, indicating at this stage the anodic current has a significant effect on the corrosion morphology instead of the corrosion rate. This is in agreement with the results of electrochemical test. Under the condition of large anodic current, the corrosion products mainly consist of two layers; FeOOH in outer layer [21,22] and Fe_3O_4 in inner layer [23], shown in Fig. 8 and Fig. 9. The pitting corrosion occurs under the inner layer because of the good adhesiveness and electro-conductivity of Fe_3O_4.

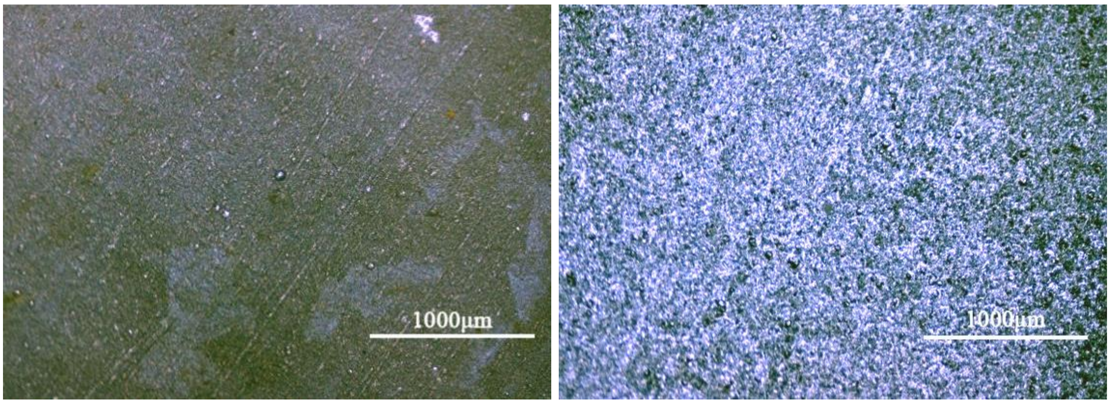

(a) 0 (b) 10mA/cm^2

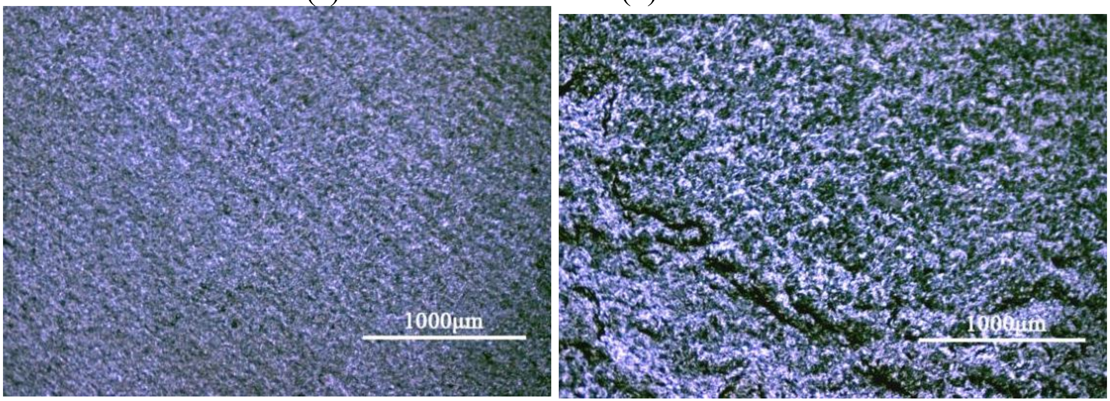

(c) 20mA/cm^2 (d) 50mA/cm^2

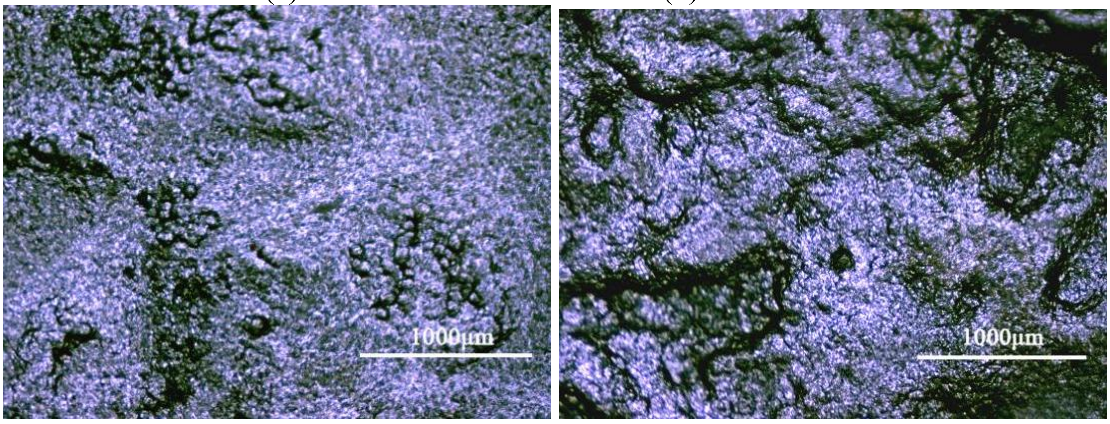

(e) 75mA/cm^2 (f) 100mA/cm^2

Figure 7. Corrosion morphology of X80 steel under different anodic current densities (0~100 mA/cm^2) in NS4 solution

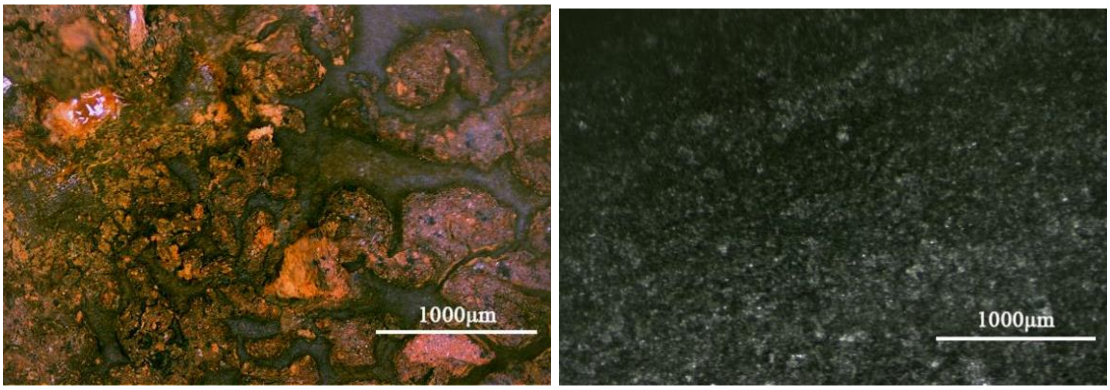

(a) Outer layer (b) Inner layer

Figure 8. Corrosion products of inner / outer rust layer at I_{ac}=100mA/cm^2 in NS4 solution

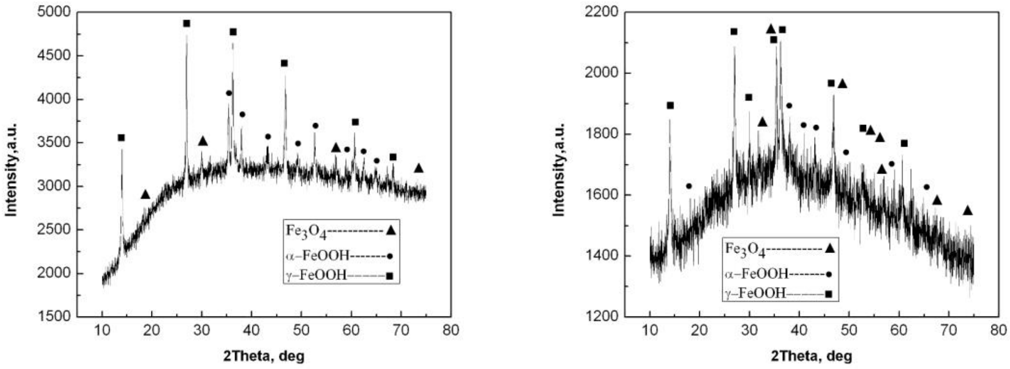

(a) 20mA/cm^2 (b) 100mA/cm^2

Figure 9. Analysis of corrosion products at I_{ac}=20mA/cm^2 and I_{ac}=100mA/cm^2 in NS4 solution

The influence of anodic current on X80 steel can be described as follows. At low anodic current density, corrosion behavior met with the Tafel's law, illustrating $Fe \rightarrow Fe^{2+}+2e^-$ [24,25]. With the increasing anodic current, the electrochemical reaction occurs in sequence: $Fe+H_2O \leftrightharpoons (FeOH)_{ad}+H^++e^-$, $(FeOH)_{ad} \rightarrow FeOH^++e^-$, $FeOH^++H^+ \leftrightharpoons Fe^{2+}+H_2O$. Once the anodic current density reaches the 75~100mA/cm^2, the double layer has formed by $2Fe^{2+}+O_2+2H_2O \rightarrow 2FeOOH+2H^+$ and $FeOOH+Fe^{2+}+2OH^- \rightarrow Fe_3O_4+2H_2O$ [26].

4. CONCLUSIONS

In this paper, the corrosion behavior of X80 steel influenced by anodic current density in NS4 solution was investigated with the following conclusions:

(1) From the results of electrochemical tests, the anodic current density mainly affects the cathodic process of X80 steel and the influence on X80 steel can be divided into two stages. The first stage occurs at lower anodic current densities, I_{ac}=5~20mA/cm^2. In this stage, the corrosion potential and corrosion current density of X80 steel increase linearly with the increase of anodic current density, evidenced by the formation of a characteristic double capacitive reactance, which is mainly formed by

an electric double layer and diffusion layer. The second stage, I_{ac}≥50mA/cm^2, shows the electric double layer and diffusion layer have been formed, and has the characteristics of a single capacitive reactance, with the corrosion rate basically unchanged.

(2) X80 steel corrosion is mostly uniform in the range I_{ac}=5~20mA/cm^2 and consists primarily of FeOOH. At higher anodic current densities in the range I_{ac}=50~100mA/cm^2, the inner corrosion products are primarily black Fe_3O_4 and the uniform corrosion gradually changes to pitting corrosion. These results are in good agreement with the electrochemical results.

References

1. Y. Gong, C.L. Xue, Z.L. Yuan, Y.X. Li and F.P. Dawalibi, *J. Power. Energy. Eng.*, 332(2015)3.
2. F.Z. Zhang, B. Luo, G.L. Wang, Y.F. Liao and L. Luo, *IEEE T. Dielect. El. In.*, 2937(2015)22.
3. P. Nicholson, *NACE International*, 10102(2010).
4. L.Y. Xu and Y.F. Cheng, *Corros. Sci.*, 150(2013)73.
5. C.F. Zhu, R. Xie and J.H. Xue, *Electrochim. Acta*, 5828(2011)56.
6. L.Y. Xu, X. Su, Z.X. Yin, Y. H. Tang and Y. F. Cheng, *Corros. Sci.*, 61(2012)215.
7. C. Yang, J.L. Li, Z.L. Li, S.X. Zhang, L. Dai and C.B. Zhang, *Corros. Rev.*, 37(2019)273.
8. C. Yang, G. Cui, Z.L. Li, Y.L. Zhao and C.B. Zhang, *Int. J. Electrochem. Sci.*, 10(2015)10223.
9. S. Qian and Y.F. Cheng, *Constr. Build. Mater.,* 148(2017)675.
10. X. Zhang, J.X. Zhang, N.W. Dai, Y. Yang, X.J. Yuan, F.H. Cao and J.Q. Zhang, *Mater. Chem. Phys.,* 206(2018)232.
11. F. Brichau, J. Deconinck and T. Driesens, *Corrosion,* 52(1996)480.
12. M. Kendig, F. Mansfeld and S. Tsai, *Corros. Sci.*, 317(1983)23.
13. C. Pérez, A. Collazo, M. Izquierdo, P. Merino and X.R. Novoa, *Prog. Org. Coat.*, 36(1999)102.
14. E.P.M. Van Westing, G.M. Ferrari and J.H.W. de Wit, *Corros. Sci.*, 39(1994)957.
15. A. Husain, J. Chakkamalayath and S. Al-Baha, *Eng. Fail. Anal.*, 82(2017)765.
16. J.W. Oldield and W.H. Sutton, *Br. Corros. J.*, 13(1989)104.
17. J.W. Oldield and W.H. Sutton, *Br. Corros. J.*, 13(1978)13.
18. C.G. Oliveira and M.G.S. Ferreira, *Corros. Sci.*, 123(2003)45.
19. L. Caceres, T. Vargas and M. Parra, *Electrochim. Acta*, 7435(2009)54.
20. L. Caceres, T. Vargas and L. Herrera, *Corros. Sci.*, 971(2009)51.
21. Y. Zhang, J.W. Tian, J. Zhong and X.M. Shi, *ACS Nano*, 12(2018)10189.
22. A. Raman, S. Nasrazadani and L. Sharma, *Metallography*, 22(1989)79.
23. H. Tanaka, R. Mishima, N. Hatanaka, T. Ishikawa and T. Nakayama, *Corros. Sci.*, 78(2014)384.
24. P. Dillmann, R. Balasubramaniam and G. Beranger, *Corros. Sci.*, 44(2002)2231.
25. F.F. Eliyan, E.S. Mahdi and A. Alfantazi, *Corros. Sci.*, 58(2012)181.
26. Y. Tamaura, K. Ito and T. Katsura, *J. Chem. Soc. Dalton.*, 2(1983)189.